

Testing Technicolor Models in Top Quark Pair Production at High Energy Photon Colliders

Hong-Yi Zhou^{a,b} Yu-Ping Kuang^{a,b} Chong-Xing Yue^{a,c},

Hua Wang^{a,b}, Gong-Ru Lu^{a,c},

a. CCAST (World Laboratory), P. O. Box 8730, Beijing 100080, China

*b. Institute of Modern Physics, Tsinghua University, Beijing, 100084, P. R. of China.**

c. Physics Department, Henan Normal University, Xin Xiang, Henan 453002, P. R. of China

Abstract

We study pseudo-Goldstone boson corrections to $\gamma\gamma \rightarrow t\bar{t}$ production rates in technicolor models with and without topcolor at the $\sqrt{s} = 0.5$ and 1.5 TeV photon colliders. We find that, for reasonable ranges of the parameters, the corrections are large enough to be observable, and the corrections in models with topcolor are considerably larger than those in models without topcolor, and they are all significantly larger than the corresponding corrections in the minimal supersymmetric standard model (MSSM) with $\tan\beta \geq 1$. So that the two kinds of technicolor models and the MSSM with $\tan\beta \geq 1$ can be experimentally distinguished.

PACS Numbers: 12.60.Nz, 14.65.Ha, 13.40.-f

*Mailing address

I. Introduction

The electroweak symmetry breaking (EWSB) mechanism remains an open question in spite of the success of the standard model (SM) compared with the new LEP precision measurement data. In the SM, elementary Higgs field is assumed to be in charge of the EWSB. So far the Higgs boson is not found, and theories with elementary scalar fields suffers from the problems of triviality, unnaturalness, etc. Therefore studying EWSB mechanisms other than the simple SM Higgs sector is one of the interesting topics in current particle theory. Technicolor (TC) theory [1] is an attractive idea of dynamical EWSB which avoids the shortcomings arising from elementary scalar fields, and it has been enlarged to the extended technicolor (ETC) theory [2] for giving masses not only to the weak gauge bosons but also to quarks and leptons. A series of improved ideas, such as walking technicolor (WTC) theory [3] [4], multiscale walking technicolor theory [5], and topcolor-assisted technicolor (TOPCTC) theory [6], have been proposed to overcome the phenomenological difficulties in the ETC theory, and these make the theory one of the important candidates of promising mechanisms for EWSB. It is thus interesting to study the effects of this kind of theory in various physical processes and see if they can be experimentally tested. It is important to notice that in most of the currently interesting improved TC models, the TC sectors are non-minimal, i.e. they all contain certain pseudo Goldstone bosons (PGB's) in the few hundred GeV region. This can be seen as the characteristic features of this kind of models. Thus studying the effects of the PGB's in processes at high energy colliders will be of special interest.

The recently discovered top quark is the heaviest particle yet experimentally found. Its mass, $m_t = 176$ GeV [7], is of the order of the EWSB scale $v = (\sqrt{2}G_F)^{-1/2} = 246$ GeV. This means that the top quark couples rather strongly to the EWSB sector so that the effects from new physics would be more apparent in processes with the top quark than with any other light quarks. Experimentally, it is possible to separately measure various production

and decay form factors of the top quark at the level of a few percent [8]. Thus theoretical calculations of various corrections to the production and decay of the top quarks are of much interest.

Top quark pair can be produced at various high energy colliders. Of special interest is to examine the ability of the suggested future TeV energy photon colliders in probing the EWSB mechanism via $t\bar{t}$ production. This paper is devoted to this kind of study. There have been various studies of probing the EWSB mechanism via top quark pair productions at high energy colliders. For example, model-independent studies [9], studies of the top quark pair production cross sections in photon collisions in the SM, the two-Higgs-doublet model, and the minimal supersymmetric SM (MSSM) [10] [11] [12], and the study of PGB contributions to the $t\bar{t}$ production cross sections at the Fermilab Tevatron [13] and the CERN LHC in a topcolor-assisted multiscale technicolor model (TOPCMTC) [14] [15], etc. The results in Ref. [15] show that PGB's do give significant contributions to the $t\bar{t}$ production cross section from which the color-octet neutral technipion and the neutral top-pion with mass close to 350 GeV can be clearly tested at the LHC and the Tevatron for reasonable range of the parameters in the TOPCMTC model. In this paper we study the PGB contributions to the $\gamma\gamma \rightarrow t\bar{t}$ cross section at the $\sqrt{s} = 0.5$ and 1.5 TeV photon colliders in various technicolor models. We shall show that, for reasonable values of the parameters in the models, the PGB contributions are quite large in models assisted by topcolor, and are considerably smaller in models without topcolor. All these cross sections are significantly larger than those in the MSSM for $\tan\beta \geq 1$ [12]. So that different models can be distinguished by the $\gamma\gamma \rightarrow t\bar{t}$ cross section measurement at the high energy photon colliders. At the $\sqrt{s} = 1.5$ TeV photon collider, even the original TOPCTC model and the TOPCMTC model can be experimentally distinguished.

This paper is organized as follows. In Sec.II, we take the Appelquist-Terning one-family

WTC model [4] as a typical example of the reasonable TC models without assisted by topcolor, and present the results of the PGB contributions to the $\gamma\gamma \rightarrow t\bar{t}$ cross section at the $\sqrt{s} = 0.5$ and 1.5 TeV photon colliders in this model. Sec.III contains the corresponding results of two typical TOPCTC models, namely the original TOPCTC model by Hill [6] and the TOPCMTC model [14] [15]. Discussions and conclusions are given in Sec.IV, and the analytic formulae for the form factors in the production amplitudes in terms of the well known standard notions of one-loop Feynman integrals [16] are presented in the APPENDIX.

II. $t\bar{t}$ production cross section in the one family WTC model

In this section, we take the Appelquist-Terning one-family WTC model [4] as a typical example of reasonable TC models without assisted by topcolor to calculate the $\gamma\gamma \rightarrow t\bar{t}$ cross section. In this model, the technilepton sector does not respect the custodial symmetry $SU(2)_c$ which makes the the oblique correction parameter S [17] small as required by the experiment. The TC group in this model is taken to be $SU(2)_{TC}$ which minimizes the S parameter. There are 36 TC PGB's composed of weak $SU(2)_W$ doublets of techniquarks Q and technileptons L . The relevant PGB's in this study are the color-octet Π_a^0 [$SU(2)_W$ -singlet] and Π_a^α [$SU(2)_W$ -triplet] composed of the techniquarks Q^\dagger (the color-singlet PGB's in this model are mainly composed of technileptons L , so that they are irrelevant to the $t\bar{t}$ production). The decay constants of these PGB's is $F_Q = 140$ GeV [4]. The masses of these PGB's are model dependent [4]. In Ref. [4], the mass of Π_a^α is taken to be in the range $250 \text{ GeV} < m_a^\alpha < 500 \text{ GeV}$. We shall also take the mass of Π_a^0 in the same range in our calculation.

[†]These PGB's are the ones denoted by Θ_a^0 and Θ_a^α in Ref. [4].

The relevant Feynman diagrams for the corrections to the $\gamma\gamma \rightarrow t\bar{t}$ production amplitudes in the Appelquist-Terning model are shown in Fig.1(a)-(n). The Feynman rules needed in the calculations can be found in Ref. [18]. For instance, the PGB-top (bottom) interactions are

$$\frac{\sqrt{2}m_t}{f_Q}(i\bar{t}\gamma_5\frac{\lambda^a}{2}t\Pi_a^0 + i\bar{t}\gamma_5\frac{\lambda^a}{2}t\Pi_a^3 + \frac{1}{\sqrt{2}}\bar{t}(1 - \gamma_5)\frac{\lambda^a}{2}b\Pi_a^+ + \frac{1}{\sqrt{2}}\bar{b}(1 + \gamma_5)\frac{\lambda^a}{2}t\Pi_a^-). \quad (1)$$

In our calculation, we use dimensional regularization to regulate all the ultraviolet divergences in the virtual loop corrections and we adopt the on-mass-shell renormalization scheme. In that scheme, we need not consider the external top quark self energy diagrams. The renormalized amplitude for $\gamma\gamma \rightarrow t\bar{t}$ contains

$$M_{ren} = M_{ren}^{(t)} + M_{ren}^{(u)} + \Delta M^{(\Delta)}, \quad (2)$$

where the superscripts t, u stand for the t, u -channel amplitudes, respectively. $\Delta M^{(\Delta)}$ is the triangle correction of Fig.1 (n). Our notations for the momenta are: p_2 and p_1 denote the momenta of the outgoing t and \bar{t} ; p_3 and p_4 denote the momenta of the two incoming photons; $\hat{s} \equiv (p_1 + p_2)^2 = (p_3 + p_4)^2$, $\hat{t} \equiv (p_4 - p_2)^2$, and $\hat{u} \equiv (p_1 - p_4)^2$. In eq.(1), $M_{ren}^{(t)}$ is contributed by Fig.1(a)-(m), and $M_{ren}^{(u)}$ is related to $M_{ren}^{(t)}$ by

$$M_{ren}^{(u)} = M_{ren}^{(t)}(p_3 \leftrightarrow p_4, \hat{t} \rightarrow \hat{u}). \quad (3)$$

The amplitude $M_{ren}^{(t)}$ contains

$$M_{ren}^{(t)} = M_0^{(t)} + \Delta M^{(t)}, \quad (4)$$

where

$$M_{0ij}^{(t)} = -i\frac{Q_t^2 e^2}{\hat{t} - m_t^2}\epsilon^\mu(p_4)\epsilon^\nu(p_3)\bar{u}(p_2)\gamma_\mu(\gamma \cdot p_3 - \gamma \cdot p_1 + m_t)\gamma_\nu v(p_1)\delta_{ij} \quad (5)$$

is the tree-level t -channel amplitude, and $\Delta M^{(t)}$ is the PGB correction to the t -channel amplitude which contains

$$\Delta M^{(t)} = \Delta M^{self(t)} + \Delta M^{v(t)} + \Delta M^{b(t)}, \quad (6)$$

in which $\Delta M^{self(t)}$, $\Delta M^{v(t)}$, $\Delta M^{b(t)}$ are the amplitudes contributed by the PGB's in the self-energy diagrams [Figs.1(b)-(c)], the vertex diagrams [Figs. 1(d)-(i)], the box diagrams [Figs.1(j)-(m)], respectively. They are

$$\Delta M_{ij}^{self(t)} = ie^2 \epsilon^\mu(p_4) \epsilon^\nu(p_3) \bar{u}(p_2) [f_2^{self} \gamma_\mu \gamma_\nu + f_6^{self} p_{2\mu} \gamma_\nu + f_{12}^{self} \not{p}_4 \gamma_\mu \gamma_\nu] v(p_1) \delta_{ij}, \quad (7)$$

$$\begin{aligned} \Delta M_{ij}^{v(t)} = & ie^2 \epsilon^\mu(p_4) \epsilon^\nu(p_3) \bar{u}(p_2) [f_2^v \gamma_\mu \gamma_\nu + f_3^v p_{1\nu} \gamma_\mu + f_6^v p_{2\mu} \gamma_\nu \\ & + f_9^v p_{2\mu} p_{1\nu} + f_{12}^v \not{p}_4 \gamma_\mu \gamma_\nu + f_{13}^v \not{p}_4 p_{1\nu} \gamma_\mu + f_{16}^v \not{p}_4 p_{2\mu} \gamma_\nu] v(p_1) \delta_{ij}, \end{aligned} \quad (8)$$

$$\begin{aligned} \Delta M_{ij}^{b(t)} = & ie^2 \epsilon^\mu(p_4) \epsilon^\nu(p_3) \bar{u}(p_2) [f_1^b g_{\mu\nu} + f_2^b \gamma_\mu \gamma_\nu + f_3^b p_{1\nu} \gamma_\mu \\ & + f_4^b p_{1\mu} \gamma_\nu + f_5^b p_{2\nu} \gamma_\mu + f_6^b p_{2\mu} \gamma_\nu + f_7^b p_{1\mu} p_{1\nu} + f_8^b p_{1\mu} p_{2\nu} \\ & + f_9^b p_{2\mu} p_{1\nu} + f_{10}^b p_{2\mu} p_{2\nu} + f_{11}^b \not{p}_4 g_{\mu\nu} + f_{12}^b \not{p}_4 \gamma_\mu \gamma_\nu \\ & + f_{13}^b \not{p}_4 p_{1\nu} \gamma_\mu + f_{14}^b \not{p}_4 p_{1\mu} \gamma_\nu + f_{15}^b \not{p}_4 p_{2\nu} \gamma_\mu + f_{16}^b \not{p}_4 p_{2\mu} \gamma_\nu \\ & + f_{17}^b \not{p}_4 p_{1\mu} p_{1\nu} + f_{18}^b \not{p}_4 p_{1\mu} p_{2\nu} + f_{19}^b \not{p}_4 p_{2\mu} p_{1\nu} + f_{20}^b \not{p}_4 p_{2\mu} p_{2\nu}] v(p_1) \delta_{ij}, \end{aligned} \quad (9)$$

and

$$M_{ren\ ij}^{(\Delta)} = ie^2 \epsilon(p_4) \cdot \epsilon(p_3) \bar{u}(p_2) f^\Delta v(p_1) \delta_{ij}, \quad (10)$$

The explicit formulae for the form factors f 's are given in the APPENDIX.

The total cross section $\sigma(s)$ of the production of $t\bar{t}$ in $\gamma\gamma$ collisions is obtained by folding the the elementary cross section $\sigma(\hat{s})$ for the subprocess $\gamma\gamma \rightarrow t\bar{t}$ with the photon luminosity at the e^+e^- colliders given in Ref. [19], i.e.

$$\sigma(s) = \int_{2m_t/\sqrt{\hat{s}}}^{x_{max}} dz \frac{dL_{\gamma\gamma}}{dz} \sigma(\hat{s}) \quad (\gamma\gamma \rightarrow t\bar{t} \text{ at } \hat{s} = z^2 s), \quad (11)$$

where $\sqrt{s}(\sqrt{\hat{s}})$ is the e^+e^- ($\gamma\gamma$) center-of-mass energy and $dL_{\gamma\gamma}/dz$ is the photon luminosity defined as

$$\frac{dL_{\gamma\gamma}}{dz} = 2z \int_{z^2/x_{max}}^{x_{max}} \frac{dx}{x} F_{\gamma/e}(x) F_{\gamma/e}(z^2/x). \quad (12)$$

For unpolarized initial electrons and laser beams, the energy spectrum of the back-scattered photon is given by [19]

$$F_{\gamma/e}(x) = \frac{1}{D(\xi)} \left[1 - x + \frac{1}{1-x} - \frac{4x}{\xi(1-x)} + \frac{4x^2}{\xi^2(1-x)^2} \right], \quad (13)$$

with

$$D(\xi) = \left(1 - \frac{4}{\xi} - \frac{8}{\xi^2} \right) \ln(1 + \xi) + \frac{1}{2} + \frac{8}{\xi} - \frac{1}{2(1 + \xi)^2}, \quad (14)$$

where $\xi = 4E_e\omega_0/m_e^2$ in which m_e and E_e stand ,respectively, for the incident electron mass and energy, ω_0 stands for the laser-photon energy, $x = \omega/E_e$ stands for the fraction of energy of the incident electron carried by the back-scattered photon. $F_{\gamma/e}(x)$ vanishes for $x > x_{max} = \omega_{max}/E_e = \xi/(1 + \xi)$. In order to avoid the creation of e^+e^- pairs by the interaction of the incident and backscattered photons, we require $\omega_0 x_{max} \leq m_e^2/E_e$ which implies $\xi \leq 2 + 2\sqrt{2} \approx 4.8$. For the choice $\xi = 4.8$, we obtain

$$x_{max} \approx 0.83, \quad D(\xi) \approx 1.8. \quad (15)$$

In the calculation of $\sigma(\hat{s})$, instead of calculating the square of the amplitude M_{ren} analytically, we calculate the amplitudes numerically by using the method of Ref. [20]. This greatly simplifies our calculations. Care must be taken in the calculation of the form factors expressed in terms of the standard loop integrals defined in Ref. [16]. As has been discussed in Ref. [21], the formulae for the form factors given in terms of the tensor loop integrals will be ill- defined when the scattering is forwards or backwards wherein the Gram determinants of some matrices vanish and thus their inverse do not exist. This problem can be solved by taking kinematic cuts on the rapidity y and the transverse momentum p_T . In this paper, we take

$$|y| < 2.5, \quad p_T > 20 \text{ GeV}. \quad (16)$$

The cuts will also increase the relative correction [22].

In our calculation, we take $m_t = 176 \text{ GeV}$, $m_b = 4.9 \text{ GeV}$, and we take $\alpha_{em}(m_Z^2) = 128.8$ with the one-loop running formula to determine the electromagnetic fine structure constant α_{em} at the desired scale. The result of the tree-level cross sections are $\sigma_0 = 57.77 \text{ fb}$ for $\sqrt{s} = 0.5 \text{ TeV}$ and $\sigma_0 = 535.4 \text{ fb}$ for $\sqrt{s} = 1.5 \text{ TeV}$. To see the main feature of the TC PGB corrections to the cross section, we simply take $m_{\Pi_a^0} = m_{\Pi_a^3} = m_{\Pi_a^\pm} \equiv m_{\Pi_a}$ to calculate the correction $\Delta\sigma$. The values of $\Delta\sigma$, the ratio $\Delta\sigma/\sigma_0$, and the total cross section $\sigma = \sigma_0 + \Delta\sigma$ for $250 \text{ GeV} \leq m_{\Pi_a} \leq 500 \text{ GeV}$ are listed in Table I. We see that for $\sqrt{s} = 0.5 \text{ TeV}$, the relative correction $\Delta\sigma/\sigma_0$ is of the order of ten percent which is about one order of magnitude larger than that in the MSSM with $\tan\beta \geq 1$ (which is about one percent) [12]. For $\sqrt{s} = 1.5 \text{ TeV}$, the relative corrections are around $(4 - 10)\%$ which is also larger than that in the MSSM with $\tan\beta \geq 1$.

For estimating the event rates, let us take an integrated luminosity of

$$\begin{aligned} \int \mathcal{L} dt &= 50 \text{ fb}^{-1}, & \text{for } \sqrt{s} = 0.5 \text{ TeV}, \\ \int \mathcal{L} dt &= 100 \text{ fb}^{-1}, & \text{for } \sqrt{s} = 1.5 \text{ TeV}, \end{aligned} \quad (17)$$

which corresponds to a one year run at the NLC [23]. There will be about 2500 events for $\sqrt{s} = 0.5 \text{ TeV}$ and 25000 events for $\sqrt{s} = 1.5 \text{ TeV}$ according to the cross sections shown in Table I. The statistical uncertainty at 95% C.L. is then around 4% for $\sqrt{s} = 0.5 \text{ TeV}$ and 1.2% for $\sqrt{s} = 1.5 \text{ TeV}$. Therefore *this model can be experimentally distinguished from the MSSM model with $\tan\beta \geq 1$ in $\gamma\gamma \rightarrow t\bar{t}$ at the future photon collider.*[‡]

[‡]We only give here an order of magnitude estimate considering only the statistical uncertainty. Practically, the systematic error and the detection efficiency should also be taken into account which are beyond the scope of this paper.

III. $t\bar{t}$ Production cross sections in TOPCTC Models

1. The Original TOPCTC Model [6]

For TOPCTC models, we first consider the original TOPCTC model proposed by Hill [6]. In this model, there are 60 TC PGB's in the TC sector with the decay constant $f_{\Pi} = 120$ GeV and three top-pions Π_t^0 , Π_t^{\pm} in the topcolor sector with the decay constant $f_{\Pi_t} = 50$ GeV [6]. The top quark mass m_t is mainly provided by the topcolor sector, while the TC sector only provide a small portion of it, say $m'_t \sim 5 - 24$ GeV [6] [24]. The mass of the top-pion depends on a parameter in the model [6]. For reasonable values of the parameter, m_{Π_t} is around 200 GeV [6]. The prediction of the light top-pion is the characteristic feature of the TOPCTC models and this is the main difference between this kind of models and TC models without topcolor. In the following calculation, we would rather take a slightly larger range, $180 \text{ GeV} \leq m_{\Pi_t} \leq 300 \text{ GeV}$, to see its effect, and we shall take the masses of the color-singlet TC PGB's to vary in the range $100 - 325$ GeV.

The color-octet TC PGB-top (bottom) interactions are similar to eq.(1) but with m_t replaced by m'_t and f_Q replaced by f_{Π} , i.e.

$$\frac{\sqrt{2}m'_t}{f_{\Pi}}(i\bar{t}\gamma_5\frac{\lambda^a}{2}t\Pi_a^0 + i\bar{t}\gamma_5\frac{\lambda^a}{2}t\Pi_a^3 + \frac{1}{\sqrt{2}}\bar{t}(1 - \gamma_5)\frac{\lambda^a}{2}b\Pi_a^+ + \frac{1}{\sqrt{2}}\bar{b}(1 + \gamma_5)\frac{\lambda^a}{2}t\Pi_a^-). \quad (18)$$

The color-singlet TC PGB-top (bottom) interactions are [18]

$$\frac{c_t m'_t}{\sqrt{2}f_{\Pi}}(i\bar{t}\gamma_5 t\Pi^0 + i\bar{t}\gamma_5 t\Pi^3 + \frac{1}{\sqrt{2}}\bar{t}(1 - \gamma_5)b\Pi^+ + \frac{1}{\sqrt{2}}\bar{b}(1 + \gamma_5)t\Pi^-), \quad (19)$$

where $c_t = \frac{1}{\sqrt{6}}$. The interactions between the top-pions and the top (bottom) quark are [18] [15]

$$\frac{m_t - m'_t}{\sqrt{2}f_{\Pi_t}}(i\bar{t}\gamma_5 t\Pi_t^0 + \frac{1}{\sqrt{2}}\bar{t}(1 - \gamma_5)b\Pi_t^+ + \frac{1}{\sqrt{2}}\bar{b}(1 + \gamma_5)t\Pi_t^-). \quad (20)$$

The color-singlet TC PGB's and the top-pions can also couple to the two photons via triangle fermion loops. It has been shown in Ref. [25] that, at the relevant energy, the technifermion triangle loops can be approximately evaluated from the formulae for the Adler-Bell-Jackiw anomaly [26] with which the general form of the effective $\Pi - B_1 - B_2$ interaction (Π denotes the PGB's Π^0, Π^3 , B_1 and B_2 are gauge fields) is [25]

$$\frac{1}{(1 + \delta_{B_1 B_2})} \left(\frac{S_{\Pi B_1 B_2}}{4\sqrt{2}\pi^2 F_\Pi} \right) \Pi \epsilon_{\mu\nu\lambda\rho} (\partial^\mu B_1^\nu) (\partial^\lambda B_2^\rho), \quad (21)$$

where the factors $S_{\Pi B_1 B_2}$ for various cases are given in Refs. [25] and [27]. Note that the electromagnetic interaction violates $SU(2)_W$ symmetry, so that the $\Pi^3 - \gamma - \gamma$ and the $\Pi_t^0 - \gamma - \gamma$ couplings do exist [25]. For example, from Ref. [25], the $S_{\Pi^0 \gamma \gamma}$ and $S_{\Pi^3 \gamma \gamma}$ factors from the techniquark triangle loop are

$$S_{\Pi^0 \gamma \gamma} = \frac{-4e^2}{3\sqrt{6}} N_{TC}, \quad (22)$$

$$S_{\Pi^3 \gamma \gamma} = \frac{4e^2}{\sqrt{6}} N_{TC}. \quad (23)$$

For the top quark triangle loop, the simple ABJ anomaly approach is not sufficient since the top quark mass is only 176 GeV. Here we explicitly calculate the top quark triangle loop and obtain the following $\Pi_t^0 - \gamma - \gamma$ interaction

$$- \frac{Q_t^2 N_c e^2 (m_t - m'_t)}{16\pi^2 \sqrt{2} f_{\Pi_t}} (4m_t C_0) \Pi_t^0 \epsilon_{\mu\nu\lambda\rho} (\partial^\mu A^\nu) (\partial^\lambda A^\rho), \quad (24)$$

where $C_0(p_4, -p_4 - p_3, m_t, m_t, m_t)$ is the standard 3-point Feynman integral [16][§].

From the above couplings, we see that there are additional important s -channel diagrams contributing to the $t\bar{t}$ production shown in Fig.1(o)-(p). The top-pion s -channel contribution is quite large compared with those from Fig.1(a)-(n) due to their strong coupling. This makes

[§]From (19) we know that the $\Pi^0 - t - \bar{t}$ coupling is proportional to m'_t , so that the top quark triangle loop contribution to the $\Pi^0 - \gamma - \gamma$ interaction is negligibly small.

the contributions in this model quite different from those in the Appelquist- Terning model presented in the last section.

Now we calculate the s -channel amplitude $M_{ren}^{(s)}$ in Fig.1(o)-(p). First of all, The Π (Π^0 or Π^3) propagator in Fig.1(o)-(p) takes the form

$$\frac{i}{\hat{s} - m_{\Pi}^2 + im_{\Pi}\Gamma_{\Pi}}, \quad (25)$$

where $\sqrt{\hat{s}}$ is the c.m. energy and Γ_{Π} is the total width of the PGB Π which is important when $\sqrt{\hat{s}}$ is close to m_{Π}^2 (since $m_{\Pi_t} \sim 200$ GeV which is well below the $t\bar{t}$ threshold, there is no need to include the width Γ_{Π_t} in the top-pion propagator). Similar to Ref. [15], we can obtain the widths Γ_{Π^0} and Γ_{Π^3} which are

$$\Gamma_{\Pi} = \Gamma(\Pi \rightarrow g_a g_b) + \Gamma(\Pi \rightarrow b\bar{b}) + \Gamma(\Pi \rightarrow t\bar{t}), \quad \text{if } m_{\Pi} > 2m_t, \quad (26)$$

where

$$\Gamma(\Pi^0 \rightarrow g_a g_b) = \frac{\alpha_s^2 c_t^2 N_{TC}^2 m_{\Pi^0}^3}{16\pi^2 F_{\Pi}^2} \left| 1 + \frac{J(R_{\Pi^0})}{2N_{TC}} \right|^2, \quad (27)$$

$$\Gamma(\Pi^3 \rightarrow g_a g_b) = \frac{\alpha_s^2 c_t^2 m_{\Pi^3}^3}{64\pi^2 F_{\Pi}^2} |J(R_{\Pi^3})|^2, \quad (28)$$

$$\Gamma(\Pi \rightarrow b\bar{b}) = \frac{3}{16\pi} \frac{c_t^2 m_b^2 m_{\Pi}}{F_{\Pi}^2} \sqrt{1 - \frac{4m_b^2}{m_{\Pi}^2}}, \quad (29)$$

$$\Gamma(\Pi \rightarrow t\bar{t}) = \frac{3}{16\pi} \frac{c_t^2 m_t^2 m_{\Pi}}{F_{\Pi}^2} \sqrt{1 - \frac{4m_t^2}{m_{\Pi}^2}}, \quad \text{if } m_{\Pi} > 2m_t, \quad (30)$$

where [27]

$$J(R_{\Pi}) = -\frac{1}{R_{\Pi}^2} \int_0^1 \frac{dx}{x(1-x)} \ln[1 - R_{\Pi}^2 x(1-x)], \quad (31)$$

in which $R_{\Pi} \equiv \frac{m_{\Pi}}{m_t}$.

With eqs.(18)-(31), we finally get

$$\Delta M_{ij}^{(s)} = ie^2 \epsilon^{\mu}(p_4) \epsilon^{\nu}(p_3) \bar{u}(p_2) [f_{\mu\nu}^s \gamma_5] v(p_1) \delta_{ij}, \quad (32)$$

where the form factor $f_{\mu\nu}^s$ is given in the APPENDIX.

Let us first look at the contributions by different TC PGB's to the amplitude $M_{ren}^{(t,u,\Delta)}$. From eq.(18) we see that, relative to the results in the last section, the color-octet TC PGB contributions to $M_{ren}^{(t,u,\Delta)}$ from Fig.1(a)-(n) is suppressed by a factor $(\frac{m'_t/f_\Pi}{m_t/f_Q})^2$ in this model. For $m'_t \sim 20$ GeV, this factor is about 2% so that the color-octet TC PGB contributions are negligibly small in this model. From eqs.(19) and (18) we see that the color-singlet TC PGB contributions from Fig.1(a)-(n) is even smaller. For $m'_t = 20$ GeV, the top-pion contributions to $M_{ren}^{(t,u)}$ are not so small. The calculated results of $\Delta\sigma$ and $\Delta\sigma/\sigma_0$ from the contribution of $M_{ren}^{(t,u)}$ by the top-pions are listed in Table II. We see that these are slightly larger than those in Table I.

Numerical calculations show that the Π^0 and Π^3 contributions to the amplitude $M_{ren}^{(s)}$ from Fig.1(o)-(p) are also negligibly small, while the contribution from the top-pion Π_t^0 to $M_{ren}^{(s)}$ is quite large. Including this contribution, the final results of $\Delta\sigma$ and the total cross section $\sigma = \sigma_0 + \Delta\sigma$ are listed in Table III. We see that these values of $\Delta\sigma$ are considerably larger than those listed in Table I. Taking the integrated luminosity in eq.(17), we have around 1000 events for $\sqrt{s} = 0.5$ TeV and around 40000 events for $\sqrt{s} = 1.5$ TeV. The corresponding statistical uncertainties at the 95% C.L. are then 6% and 1%, respectively. Thus *this model is experimentally distinguishable from the Appelquist-Terning model and the MSSM with $\tan\beta \geq 1$ in $\gamma\gamma \rightarrow t\bar{t}$.*

2. The TOPCMTC Model [14] [15]

This model is different from the original TOPCTC model [6] mainly by the change of the TC sector in which $f_\Pi = 40$ GeV instead of the original $f_\Pi = 120$ GeV, and [14]

$$c_t = \frac{2}{\sqrt{6}}, \quad (33)$$

$$S_{\Pi^0\gamma\gamma} = \frac{10e^2}{3\sqrt{6}}N_{TC}, \quad (34)$$

$$S_{\Pi^3\gamma\gamma} = \frac{2e^2}{\sqrt{6}}N_{TC}. \quad (35)$$

Thus, relative to the results in the last section, the suppression factor $(\frac{m'_t/f_\Pi}{m_t/f_Q})^2$ of the color-octet TC PGB contribution is now 0.16 for $m'_t = 20$ GeV, so that its contribution to $M_{ren}^{(t,u,\Delta)}$ is still negligible (the relative correction is about -0.2% to 2% for $\sqrt{s} = 0.5$ TeV and -0.1% to 1% for $\sqrt{s} = 1.5$ TeV). The calculated results of the total $\Delta\sigma$ and $\sigma = \sigma_0 + \Delta\sigma$ containing the contributions of top-pion from Fig.1(a)-(p) to both $M_{ren}^{(t,u,\Delta)}$ and $M_{ren}^{(s)}$ and of Π^0 , Π^3 from Fig.1(o)-(p) to $M_{ren}^{(s)}$ for $m_\Pi \sim 100 - 325$ GeV are listed in Table IV. For $\sqrt{s} = 0.5$ TeV, we see that the values of $\Delta\sigma$ is slightly larger than those in Table III but not much. Thus the results of this model are close to those in the original TOPCTC model at $\sqrt{s} = 0.5$ TeV. For $\sqrt{s} = 1.5$ TeV, the values of $\Delta\sigma$ in Table IV are much larger than those in Table III, especially with large m'_t . To understand the reasons for such a difference, let us notice that the main difference between these two topcolor assisted TC models comes from the contributions of the PGB's Π^0 and Π^3 in the TC sector. There are three factors in eq.(11) affecting this issue: (a) in $\sigma(\hat{s})$, Π^0 and Π^3 contributions are important at large $\sqrt{\hat{s}} = m_{t\bar{t}}$ (cf. Fig.2); (b) the available range of $\sqrt{\hat{s}}$ is determined by $\min\{\sqrt{\hat{s}}\} = 2m_t = 352$ GeV and $\max\{\sqrt{\hat{s}}\} = x_{max}\sqrt{s} = 0.83\sqrt{s}$ (cf. eq.(15)), so that $\max\{\sqrt{\hat{s}}\}$ is s -dependent; (c) the $\gamma\gamma$ luminosity $\frac{dL_{\gamma\gamma}}{dz}$ decreases rapidly in the vicinity of the $\max\{\sqrt{\hat{s}}\}$ cf. eq.(12)) [28] which gives rise to a suppression of the large $\sqrt{\hat{s}}$ contributions to $\sigma(s)$. From (b) we see that the available $\sqrt{\hat{s}}$ in the case of $\sqrt{s} = 0.5$ TeV is in a narrow range of $352 - 415$ GeV which is near the $t\bar{t}$ threshold, so that the contributions of Π^0 and Π^3 are less important than that of the top-pion (cf. (a)) and the additional $\gamma\gamma$ luminosity suppression effect (c) plays a significant role in this narrow range. In the case of $\sqrt{s} = 1.5$ TeV, the available $\sqrt{\hat{s}}$ spreads in a much wider range of $352 - 1245$ GeV which increases the importance of the Π^0 and Π^3 contributions (cf. (a)) and the $\gamma\gamma$ luminosity suppression effect (c) is less significant in this wide range.

Next we look at the total cross section $\sigma(s)$. Take the case of $m_{\Pi_t} = 180$ GeV and $m_{\Pi} = 100$ GeV as an example. The relative difference between the cross sections in the two tables for $m'_t = 5$ GeV is about 6%, and for $m'_t = 20$ GeV is about 15% for $\sqrt{s} = 0.5$ TeV and 17% for $\sqrt{s} = 1.5$ TeV. These are not so significant as the differences between the values of $\Delta\sigma$. To see the observability of the difference, we look at the statistical uncertainties. Taking the integrated luminosity in eq.(17), we have 750 – 2000 events for $\sqrt{s} = 0.5$ TeV and 30000 – 40000 events for $\sqrt{s} = 1.5$ TeV according to the values of σ given in Table IV. The statistical uncertainties at the 95% C.L. are thus (4 – 7)% for $\sqrt{s} = 0.5$ TeV and around 1% for $\sqrt{s} = 1.5$ TeV. From this statistics, we first conclude that *this model can be clearly distinguished from the Appelquist- Terning model and the MSSM with $\tan\beta \geq 1$ in the $\gamma\gamma \rightarrow t\bar{t}$ experiments.* Then we consider the relative difference of σ between these two topcolor assisted models, we see that the 6% difference in the case of $m'_t = 5$ GeV can be easily observed at the $\sqrt{s} = 1.5$ TeV collider, but is hard to be observed at the $\sqrt{s} = 0.5$ TeV collider. In the case of $m'_t = 20$ GeV, the 15% and 17% differences at $\sqrt{s} = 0.5$ TeV and 1.5 TeV can all be experimentally observed. Thus *even the difference between the original TOPCTC model and the TOPCMTC model can be clearly observed in the $\gamma\gamma \rightarrow t\bar{t}$ experiment at the $\sqrt{s} = 1.5$ TeV photon collider.*

IV. Discussions and Conclusions

In this paper, we have studied the possibility of testing different currently interesting improved technicolor models in the $\gamma\gamma \rightarrow t\bar{t}$ experiments at the $\sqrt{s} = 0.5$ TeV and $\sqrt{s} = 1.5$ TeV photon colliders via the effects of their typical PGB's in the sense of the statistical uncertainty. In this calculation, we have neglected the corrections from direct TC dynamics. Now we give an order of magnitude estimate of the TC dynamics effect based on the results

in Ref. [29]. In Ref. [29], the authors considered the generation of the top quark mass via ETC with a minimal TC model containing only one-doublet of technifermions. In such a simple model, there is no PGB. The ETC dynamics was described by an effective four-fermion interaction between the technifermion and the top quark, and the coupling strength was determined by requiring that m_t is completely given by this interaction. This four-fermion interaction provides a scalar TC-hadron (with mass around 2 TeV) contribution to the $\gamma\gamma \rightarrow t\bar{t}$ cross section as a typical correction from the TC dynamics [29]. Such a TC-hadron correction only contributes in the case that the two photons are completely polarized in the same polarization [29]. So they considered only this completely polarized case in which the tree-level SM cross section (from t -channel top quark exchange) is suppressed at high energies [11]. In addition, they imposed a polar angle cut $\cos\theta_c = 0.5$ to further enhance the relative correction from the TC-hadron contribution. Their result is that the relative correction increases rapidly with the center-of-mass energy $\sqrt{\hat{s}}$: the relative correction at $\sqrt{\hat{s}} = 0.5$ TeV is negligibly small, while those at $\sqrt{\hat{s}} = 1$ and 1.5 TeV are around -8% and -43% , respectively [29]. What we have considered in this paper are the cross sections with unpolarized photons, and our polar angle cut is given in eq.(16) which corresponds to $\cos\theta_c = 0.99$. We can estimate the corresponding TC-hadron relative correction in our case as follows. We know that averaging over the photon polarizations will reduce the TC-hadron contribution since it contributes only to a special polarization. On the other hand, the change of the polar angle cut from $\cos\theta_c = 0.5$ to $\cos\theta_c = 0.99$ will increase the TC-hadron contribution. As a rough order of magnitude estimate, we simply expect that

$$\left[\Delta\sigma_{TC}^{had}\right]_{\cos\theta_c=0.99}^{unpolarized} \sim \left[\Delta\sigma_{TC}^{had}\right]_{\cos\theta_c=0.5}^{polarized}. \quad \text{Then}$$

$$\left[\frac{\Delta\sigma(\hat{s})_{TC}^{had}}{\sigma(\hat{s})_0}\right]_{\cos\theta_c=0.99}^{unpolarized} \sim \left[\frac{\Delta\sigma(\hat{s})_{TC}^{had}}{\sigma(\hat{s})_0}\right]_{\cos\theta_c=0.5}^{polarized} \cdot \frac{[\sigma(\hat{s})_0]_{\cos\theta_c=0.5}^{polarized}}{[\sigma(\hat{s})_0]_{\cos\theta_c=0.99}^{unpolarized}}. \quad (36)$$

On the R.H.S. of eq.(36), the first factor is given in Ref. [29], and the second factor can be calculated from the explicit formulae given in Ref. [11] which lead to

$[\sigma_0(\hat{s})]_{\cos\theta_c=0.5}^{pol} / [\sigma_0(\hat{s})]_{\cos\theta_c=0.99}^{unpolarized} = 0.42, 0.099, 0.039$ for $\sqrt{\hat{s}} = 0.5, 1.0,$ and 1.5 TeV, respectively. From this we see that the present relative correction $[\Delta\sigma_{TC}^{had}(\hat{s})/\sigma(\hat{s})_0]_{\cos\theta_c=0.99}^{unpolarized}$ is also negligibly small at $\sqrt{\hat{s}} = 0.5$ TeV, and those at $\sqrt{\hat{s}} = 1.0$ and 1.5 TeV are -0.8% and -1.7% , respectively. Taking the convolution (11) with the photon luminosity will not affect the order of magnitude. So that the TC-hadron relative correction is of the same order of magnitude as the MSSM corrections and is significantly smaller than the PGB corrections shown in the last two sections. Thus we see that the correction from the direct TC dynamics is at least not important in the present study** and the conclusions in the last two sections are not affected by it. Our conclusions hold in most of the currently interesting improved TC model which contain certain PGB's. TC model without PGB does not belong to this category.

In summary, our calculation shows that

- (i) corrections to the $t\bar{t}$ production cross sections in reasonable technicolor models without assisted by topcolor are large enough to be observed, and are larger than those in the MSSM with $\tan\beta \geq 1$, so that these two kinds of models are experimentally distinguishable;
- (ii) corrections to the $t\bar{t}$ production cross sections in topcolor assisted technicolor models are much larger than those in models without topcolor, and this kind of model can be clearly distinguished from models without topcolor and MSSM with $\tan\beta \geq 1$ in the $\gamma\gamma \rightarrow t\bar{t}$ experiments.
- (iii) it is even possible to distinguish the TOPCMTC model from the original TOPCTC model in the $\gamma\gamma \rightarrow t\bar{t}$ experiment at the $\sqrt{s} = 1.5$ TeV photon collider, while these two models can be distinguished at the $\sqrt{s} = 0.5$ TeV photon collider only if the parameter m'_t is as large as 20 GeV.

**In the topcolor-assisted TC models the ETC only gives rise to a small portion m'_t of the top quark mass ($m'_t \ll m_t$). So that the TC-hadron correction is even much smaller in such models.

We see that light neutral PGB contributions play an important role in the $\gamma\gamma \rightarrow t\bar{t}$ production rates. The direct detection of light neutral technipions at e^+e^- colliders has been studied in Refs. [30] [25] and the signals are not so strong; the detection at hadron colliders has been studied in Ref. [14] and the detection is more promising. The detection of the neutral top-pion has been discussed in Ref. [6] which shows that it imitates some effects of states in two-scale TC models. In Ref. [15], it is shown that a neutral top-pion peak can be seen in the $t\bar{t}$ production at the LHC only if its mass is close to 350 GeV. Our result in this paper provides an additional test of the light neutral top-pion and technipion effects through the process $\gamma\gamma \rightarrow t\bar{t}$ at the LC.

We thus conclude that the $\gamma\gamma \rightarrow t\bar{t}$ experiments at the future photon colliders are really interesting in probing the electroweak symmetry breaking mechanism.

ACKNOWLEDGMENT

This work is supported by the National Natural Science Foundation of China, the Fundamental Research Foundation of Tsinghua University, a special grant from the State Commission of Education of China, and the Natural Science Foundation of Henan Scientific Committee.

APPENDIX:

We present here the explicit formulae for the form factors appearing in eqs.(7)-(10) and (32)^{††}. The renormalization constants are

^{††}Here we have corrected some typographical mistakes in the form factors given in a previous paper [31].

$$Z^k = B_1(p, m'_k, m_k)|_{p^2=m_t^2} + 2m_t^2 \frac{\partial^2}{\partial p^2} (-Y_k B_0 + B_1)(p, m'_k, m_k)|_{p^2=m_t^2}, \quad (\text{A1})$$

$$\delta m^k = m_t [Y_k B_0 - B_1](p, m'_k, m_k)|_{p^2=m_t^2}. \quad (\text{A2})$$

$$f_2^{self(b)(c)} = \frac{Q_t^2}{(m_t^2 - \hat{t})^2} \sum_{k=\Pi_t^0, \Pi_a^0, \Pi_a^3, \Pi_t^+, \Pi_a^+} q_k \{2p_2 \cdot p_4 [m_t (-Y_k B_0 + Z^k) + \delta m^k + m_t (B_1 - Z^k)]\}, \quad (\text{A3})$$

$$f_6^{self(b)(c)} = \frac{Q_t^2}{(m_t^2 - \hat{t})^2} \sum_{k=\Pi_t^0, \Pi_a^0, \Pi_a^3, \Pi_t^+, \Pi_a^+} q_k \{-4m_t [m_t (-Y_k B_0 + Z^k) + \delta m^k] - 4m_t^2 (B_1 - Z^k) + 4p_2 \cdot p_4 (B_1 - Z^k)\}, \quad (\text{A4})$$

$$f_{12}^{self(b)(c)} = \frac{1}{2} f_6^{self(b)(c)}, \quad (\text{A5})$$

where $B_0, B_1(t, m'_k, m_k)$ are 2-point Feynman integrals [16], the superscripts (b), (c) indicate the labels in Fig.1 .

$$f_2^{v(d)(e)} = \frac{Q_t}{\hat{t} - m_t^2} \sum_{k=\Pi_t^0, \Pi_a^0, \Pi_a^3, \Pi_t^+, \Pi_a^+} Q'_k q_k [-2p_2 \cdot p_4 (m_t (C_0 + C_{11}) + m'_k Y_k C_0)], \quad (\text{A6})$$

$$f_6^{v(d)(e)} = \frac{Q_t}{\hat{t} - m_t^2} \sum_{k=\Pi_t^0, \Pi_a^0, \Pi_a^3, \Pi_t^+, \Pi_a^+} Q'_k q_k [1 - 4C_{24} - 2Z^k + m_t^2 (2C_0 + 4C_{11} + 2C_{21}) + 2m_k'^2 C_0 + 4m_t m'_k Y_k (C_0 + C_{11})], \quad (\text{A7})$$

$$f_{12}^{v(d)(e)} = \frac{Q_t}{\hat{t} - m_t^2} \sum_{k=\Pi_t^0, \Pi_a^0, \Pi_a^3, \Pi_t^+, \Pi_a^+} Q'_k q_k [\frac{1}{2} - 2C_{24} - Z^k + 2p_2 \cdot p_4 (C_{12} + C_{23}) + m_t^2 (C_0 - C_{21}) + m_k'^2 C_0 + 2m_t m'_k Y_k C_0], \quad (\text{A8})$$

$$f_{16}^{v(d)(e)} = \frac{Q_t}{\hat{t} - m_t^2} \sum_{k=\Pi_t^0, \Pi_a^0, \Pi_a^3, \Pi_t^+, \Pi_a^+} Q'_k q_k [-2m_t (C_{11} + C_{21}) - 2m'_k Y_k C_{11}], \quad (\text{A9})$$

where $C_0, C_{lm}(-p_2, p_4, m_k, m'_k, m'_k)$ are 3-point Feynman integrals.

$$f_6^{v(f)} = \frac{Q_t}{\hat{t} - m_t^2} \sum_{k=\Pi_t^+, \Pi_a^+} q_k [-4C_{24} - 2Z^k + 4p_2 \cdot p_4 (C_{12} + C_{23}) - 4m_t^2 (C_{11} + C_{21})], \quad (\text{A10})$$

$$f_{12}^{v(f)} = \frac{Q_t}{\hat{t} - m_t^2} \sum_{k=\Pi_t^+, \Pi_a^+} q_k [-2C_{24} - Z^k], \quad (\text{A11})$$

$$f_{16}^{v(f)} = \frac{Q_t}{\hat{t} - m_t^2} \sum_{k=\Pi_t^+, \Pi_a^+} q_k [2m_t (C_{11} + C_{21})], \quad (\text{A12})$$

where $C_0, C_{lm}(-p_2, p_4, m_b, m_k, m_k)$ are 3-point Feynman integrals.

$$f_2^{v(g)(h)} = \frac{Q_t}{\hat{t} - m_t^2} \sum_{k=\Pi_t^0, \Pi_a^0, \Pi_a^3, \Pi_t^+, \Pi_a^+} Q'_k q_k [-2m_t p_2 \cdot p_4 (C_0 + C_{11}) - 2m'_k p_2 \cdot p_4 Y_k C_0], \quad (\text{A13})$$

$$f_3^{v(g)(h)} = \frac{Q_t}{\hat{t} - m_t^2} \sum_{k=\Pi_t^0, \Pi_a^0, \Pi_a^3, \Pi_t^+, \Pi_a^+} Q'_k q_k [4p_2 \cdot p_4 (C_{12} + C_{23})], \quad (\text{A14})$$

$$f_6^{v(g)(h)} = \frac{Q_t}{\hat{t} - m_t^2} \sum_{k=\Pi_t^0, \Pi_a^0, \Pi_a^3, \Pi_t^+, \Pi_a^+} Q'_k q_k [1 - 4C_{24} - 2Z^k + 4p_2 \cdot p_4 (C_{12} + C_{23}) + m_t^2 (2C_0 - 2C_{21}) + 2m_k'^2 C_0 + 4m_t m'_k Y_k C_0], \quad (\text{A15})$$

$$f_9^{v(g)(h)} = \frac{Q_t}{\hat{t} - m_t^2} \sum_{k=\Pi_t^0, \Pi_a^0, \Pi_a^3, \Pi_t^+, \Pi_a^+} Q'_k q_k [-4m_t (C_{11} + C_{21})], \quad (\text{A16})$$

$$f_{12}^{v(g)(h)} = \frac{1}{2} f_6^{v(g)(h)}, \quad (\text{A17})$$

$$f_{13}^{v(g)(h)} = \frac{1}{2} f_9^{v(g)(h)}, \quad (\text{A18})$$

where $C_0, C_{lm}(p_1, -p_3, m_k, m'_k, m'_k)$ are 3-point Feynman integrals.

$$f_3^{v(i)} = \frac{Q_t}{\hat{t} - m_t^2} \sum_{k=\Pi_t^+, \Pi_a^+} q_k [-4p_2 \cdot p_4 (C_{12} + C_{23})], \quad (\text{A19})$$

$$f_6^{v(i)} = \frac{Q_t}{\hat{t} - m_t^2} \sum_{k=\Pi_t^+, \Pi_a^+} q_k [-4C_{24} - 2Z^k], \quad (\text{A20})$$

$$f_9^{v(i)} = \frac{Q_t}{\hat{t} - m_t^2} \sum_{k=\Pi_t^+, \Pi_a^+} q_k [4m_t (C_{11} + C_{21})], \quad (\text{A21})$$

$$f_{12}^{v(i)} = \frac{1}{2} f_6^{v(i)}, \quad (\text{A22})$$

$$f_{13}^{v(i)} = \frac{1}{2} f_9^{v(i)}, \quad (\text{A23})$$

where $C_0, C_{lm}(p_1, -p_3, m_b, m_k, m_k)$ are 3-point Feynman integrals.

$$f_1^{b(j)(k)} = \sum_{k=\Pi_t^0, \Pi_a^0, \Pi_a^3, \Pi_t^+, \Pi_a^+} Q_k'^2 q_k [4m_t (D_{27} + D_{311}) + 4m'_k Y_k D_{27}], \quad (\text{A24})$$

$$f_2^{b(j)(k)} = \sum_{k=\Pi_t^0, \Pi_a^0, \Pi_a^3, \Pi_t^+, \Pi_a^+} Q_k'^2 q_k [-m_t^3 D_{31} + 2m_t (p_2 \cdot p_4 D_{34} + p_2 \cdot p_3 D_{35} - p_3 \cdot p_4 D_{310} - 3D_{311}) - 6m_t D_{27} - m_t^3 (3D_{21} + 3D_{11} + D_0) + 2m_t p_2 \cdot p_4 (D_{21} + 2D_{24} - D_{25} + D_{11} + D_{12} - D_{13}) + 2m_t p_2 \cdot p_3 D_{25} - 2m_t p_3 \cdot p_4 D_{26} + m_t m_k'^2 (D_0 + D_{11}) + m'_k Y_k [(m_k'^2 - m_t^2) D_0 - m_t^2 (2D_{11} + D_{21})]$$

$$\begin{aligned}
& +2p_2 \cdot p_4 (D_{11} + D_{12} - D_{13} + D_{24}) + 2p_2 \cdot p_3 D_{25} - 2p_3 \cdot p_4 D_{26} - 4D_{27}], \\
f_3^{b(j)(k)} = & \sum_{k=\Pi_t^0, \Pi_a^0, \Pi_a^3, \Pi_t^+, \Pi_a^+} Q_k'^2 q_k [2m_t^2 D_{12} - 2m_k'^2 D_{12} - 2m_t^2 D_{13} \\
& + 2m_k'^2 D_{13} + 4m_t^2 D_{23} + 4m_t^2 D_{24} - 4m_t^2 D_{25} - 4m_t^2 D_{26} + 4D_{27} \\
& - 4m_t^2 D_{33} + 2m_t^2 D_{34} - 2m_t^2 D_{35} + 4m_t^2 D_{37} + 4m_t^2 D_{39} - 4m_t^2 D_{310} \\
& + 8D_{312} - 12D_{313} + p_2 \cdot p_4 (-4D_{22} - 8D_{23} + 4D_{25} + 8D_{26} + 4D_{33} - 4D_{36} \\
& - 4D_{37} + 4D_{38} - 8D_{39} + 8D_{310}) + p_1 \cdot p_4 (-4D_{23} + 4D_{26} + 4D_{33} + 4D_{38} - 8D_{39}) \\
& + p_1 \cdot p_2 (4D_{23} - 4D_{26} - 4D_{33} + 4D_{37} + 4D_{39} - 4D_{310})], \tag{A26}
\end{aligned}$$

$$\begin{aligned}
f_4^{b(j)(k)} = & \sum_{k=\Pi_t^0, \Pi_a^0, \Pi_a^3, \Pi_t^+, \Pi_a^+} Q_k'^2 q_k [-2m_t^2 D_{13} - 2m_k'^2 D_{13} + 4m_t^2 D_{33} + 2m_t^2 D_{35} \\
& - 4m_t^2 D_{37} + 8D_{313} + p_2 \cdot p_4 (4D_{23} - 4D_{25} - 4D_{33} + 4D_{37} + 4D_{39} - 4D_{310}) \\
& + p_1 \cdot p_4 (-4D_{33} + 4D_{39}) + p_1 \cdot p_2 (4D_{33} - 4D_{37}) - 4m_t m_k' Y_k D_{13}], \tag{A27}
\end{aligned}$$

$$\begin{aligned}
f_5^{b(j)(k)} = & \sum_{k=\Pi_t^0, \Pi_a^0, \Pi_a^3, \Pi_t^+, \Pi_a^+} Q_k'^2 q_k [-2m_t^2 D_{11} + 2m_k'^2 D_{11} \\
& + 2m_t^2 D_{12} - 2m_k'^2 D_{12} - 4m_t^2 D_{21} + 4m_t^2 D_{24} + 4m_t^2 D_{25} \\
& - 4m_t^2 D_{26} - 2m_t^2 D_{31} + 2m_t^2 D_{34} + 4m_t^2 D_{35} - 4m_t^2 D_{37} \\
& + 4m_t^2 D_{39} - 4m_t^2 D_{310} - 8D_{311} + 8D_{312} \\
& + p_2 \cdot p_4 (-4D_{22} + 4D_{24} - 4D_{25} + 4D_{26} + 4D_{34} - 4D_{35} - 4D_{36} \\
& + 4D_{37} + 4D_{38} - 4D_{39}) + p_1 \cdot p_4 (-4D_{25} + 4D_{26} + 4D_{37} + 4D_{38} - 4D_{39} - 4D_{310}) \\
& + p_1 \cdot p_2 (+4D_{25} - 4D_{26} + 4D_{35} - 4D_{37} + 4D_{39} - 4D_{310})], \tag{A28}
\end{aligned}$$

$$\begin{aligned}
f_6^{b(j)(k)} = & \sum_{k=\Pi_t^0, \Pi_a^0, \Pi_a^3, \Pi_t^+, \Pi_a^+} Q_k'^2 q_k [2m_t^2 D_0 + 2m_k'^2 D_0 + 4m_t^2 D_{11} \\
& - 4m_t^2 D_{13} + 2m_t^2 D_{21} - 4m_t^2 D_{25} + 4D_{311} - 4D_{313} \\
& + p_1 \cdot p_4 (4D_{25} - 4D_{26}) + 4m_t m_k' Y_k (D_0 + D_{11} - D_{13})], \tag{A29}
\end{aligned}$$

$$f_7^{b(j)(k)} = \sum_{k=\Pi_t^0, \Pi_a^0, \Pi_a^3, \Pi_t^+, \Pi_a^+} Q_k'^2 q_k [4m_t (D_{26} + D_{310}) + 4m_k' Y_k D_{26}], \tag{A30}$$

$$f_8^{b(j)(k)} = \sum_{k=\Pi_t^0, \Pi_a^0, \Pi_a^3, \Pi_t^+, \Pi_a^+} Q_k'^2 q_k [4m_t (-D_{25} + D_{26} - D_{35} + D_{310}) + 4m_k' Y_k (D_{26} - D_{25})], \tag{A31}$$

$$f_9^{b(j)(k)} = \sum_{k=\Pi_t^0, \Pi_a^0, \Pi_a^3, \Pi_t^+, \Pi_a^+} Q_k'^2 q_k [4m_t(-D_{12} - 2D_{24} + D_{26} - D_{34} + D_{310}) + 4m_k' Y_k(D_{26} - D_{24} - D_{12})], \quad (\text{A32})$$

$$f_{10}^{b(j)(k)} = \sum_{k=\Pi_t^0, \Pi_a^0, \Pi_a^3, \Pi_t^+, \Pi_a^+} Q_k'^2 q_k [4m_t(D_{11} - D_{12} + 2D_{21} - 2D_{24} - D_{25} + D_{26} + D_{31} - D_{34} - D_{35} + D_{310}) + 4m_k' Y_k(D_{11} - D_{12} + D_{21} - D_{24} - D_{25} + D_{26})], \quad (\text{A33})$$

$$f_{11}^{b(j)(k)} = \sum_{k=\Pi_t^0, \Pi_a^0, \Pi_a^3, \Pi_t^+, \Pi_a^+} Q_k'^2 q_k [-4D_{27} - 4D_{312} + 4D_{313}], \quad (\text{A34})$$

$$f_{12}^{b(j)(k)} = \sum_{k=\Pi_t^0, \Pi_a^0, \Pi_a^3, \Pi_t^+, \Pi_a^+} Q_k'^2 q_k [m_t^2(D_{34} - D_{35}) + 2[p_2 \cdot p_4(D_{310} - D_{36}) + p_2 \cdot p_3(D_{37} - D_{310}) + p_3 \cdot p_4(D_{38} - D_{39}) + 4D_{312} - 4D_{313} + 2D_{27}] + m_t^2(2D_{24} - 2D_{25} - D_{21}) + 2[p_2 \cdot p_4(D_{25} + 2D_{26} - D_{22} - D_{23}) + p_2 \cdot p_3 D_{25} - p_3 \cdot p_4 D_{26}] + m_t^2(D_0 + D_{12} - D_{13}) + m_k'^2(D_0 - D_{12} + D_{13}) + 2m_t m_k' Y_k D_0], \quad (\text{A35})$$

$$f_{13}^{b(j)(k)} = \sum_{k=\Pi_t^0, \Pi_a^0, \Pi_a^3, \Pi_t^+, \Pi_a^+} Q_k'^2 q_k [-2m_t(D_{11} + D_{24}) - 2m_k' Y_k D_{13}], \quad (\text{A36})$$

$$f_{14}^{b(j)(k)} = \sum_{k=\Pi_t^0, \Pi_a^0, \Pi_a^3, \Pi_t^+, \Pi_a^+} Q_k'^2 q_k [2m_t(D_{13} + D_{25}) + 2m_k' Y_k D_{13}], \quad (\text{A37})$$

$$f_{15}^{b(j)(k)} = \sum_{k=\Pi_t^0, \Pi_a^0, \Pi_a^3, \Pi_t^+, \Pi_a^+} Q_k'^2 q_k [2m_t(D_{11} - D_{12} + D_{21} - D_{24}) + 2m_k' Y_k(D_{11} - D_{12})], \quad (\text{A38})$$

$$f_{16}^{b(j)(k)} = \sum_{k=\Pi_t^0, \Pi_a^0, \Pi_a^3, \Pi_t^+, \Pi_a^+} Q_k'^2 q_k [2m_t(-D_{11} + D_{13} - D_{21} + D_{25}) + 2m_k' Y_k(D_{13} - D_{11})], \quad (\text{A39})$$

$$f_{17}^{b(j)(k)} = 4 \sum_{k=\Pi_t^0, \Pi_a^0, \Pi_a^3, \Pi_t^+, \Pi_a^+} Q_k'^2 q_k [D_{23} - D_{26} - D_{38} + D_{39}], \quad (\text{A40})$$

$$f_{18}^{b(j)(k)} = 4 \sum_{k=\Pi_t^0, \Pi_a^0, \Pi_a^3, \Pi_t^+, \Pi_a^+} Q_k'^2 q_k [D_{25} - D_{26} - D_{37} - D_{38} + D_{39} + D_{310}], \quad (\text{A41})$$

$$f_{19}^{b(j)(k)} = 4 \sum_{k=\Pi_t^0, \Pi_a^0, \Pi_a^3, \Pi_t^+, \Pi_a^+} Q_k'^2 q_k [D_{22} + D_{23} - D_{25} - D_{26} + D_{36} - D_{38} + D_{39} - D_{310}], \quad (\text{A42})$$

$$f_{20}^{b(j)(k)} = 4 \sum_{k=\Pi_t^0, \Pi_a^0, \Pi_a^3, \Pi_t^+, \Pi_a^+} Q_k'^2 q_k [D_{22} - D_{24} + D_{25} - D_{26} - D_{34} + D_{35} + D_{36} - D_{37} - D_{38} + D_{39}], \quad (\text{A43})$$

where $D_0, D_{lm}, D_{lmn}(-p_2, p_4, p_3, m_k, m_k', m_k', m_k')$ are 4-point Feynman integrals.

$$f_1^{b(l)} = \sum_{k=\Pi_t^+, \Pi_a^+} q_k [-4m_t D_{311}], \quad (\text{A44})$$

$$f_2^{b(l)} = 0, \quad (\text{A45})$$

$$f_3^{b(l)} = 4 \sum_{k=\Pi_t^+, \Pi_a^+} q_k [D_{27} + D_{312}], \quad (\text{A46})$$

$$f_4^{b(l)} = 4 \sum_{k=\Pi_t^+, \Pi_a^+} q_k [D_{313}], \quad (\text{A47})$$

$$f_5^{b(l)} = 4 \sum_{k=\Pi_t^+, \Pi_a^+} q_k [-D_{311} + D_{312}], \quad (\text{A48})$$

$$f_6^{b(l)} = 4 \sum_{k=\Pi_t^+, \Pi_a^+} q_k [-D_{27} - D_{311} + D_{313}], \quad (\text{A49})$$

$$f_7^{b(l)} = -4m_t \sum_{k=\Pi_t^+, \Pi_a^+} q_k [D_{25} + D_{310}], \quad (\text{A50})$$

$$f_8^{b(l)} = 4m_t \sum_{k=\Pi_t^+, \Pi_a^+} q_k [D_{35} - D_{310}], \quad (\text{A51})$$

$$f_9^{b(l)} = 4m_t \sum_{k=\Pi_t^+, \Pi_a^+} q_k [D_{11} + D_{21} + D_{24} - D_{25} + D_{34} - D_{310}], \quad (\text{A52})$$

$$f_{10}^{b(l)} = 4m_t \sum_{k=\Pi_t^+, \Pi_a^+} q_k [-D_{21} + D_{24} - D_{31} + D_{34} + D_{35} - D_{310}], \quad (\text{A53})$$

$$f_{11}^{b(l)} = \sum_{k=\Pi_t^+, \Pi_a^+} q_k [4D_{312} - 4D_{313}], \quad (\text{A54})$$

$$f_{12}^{b(l)} = f_{13}^{b(l)} = f_{14}^{b(l)} = f_{15}^{b(l)} = f_{16}^{b(l)} = 0, \quad (\text{A55})$$

$$f_{17}^{b(l)} = 4 \sum_{k=\Pi_t^+, \Pi_a^+} q_k [-D_{23} + D_{26} + D_{38} - D_{39}], \quad (\text{A56})$$

$$f_{18}^{b(l)} = 4 \sum_{k=\Pi_t^+, \Pi_a^+} q_k [D_{37} + D_{38} - D_{39} - D_{310}], \quad (\text{A57})$$

$$f_{19}^{b(l)} = 4 \sum_{k=\Pi_t^+, \Pi_a^+} q_k [-D_{12} + D_{13} - D_{22} - D_{23} - D_{24} + D_{25} + 2D_{26} - D_{36} + D_{38} - D_{39} + D_{310}], \quad (\text{A58})$$

$$f_{20}^{b(l)} = 4 \sum_{k=\Pi_t^+, \Pi_a^+} q_k [-D_{22} + D_{24} - D_{25} + D_{26} + D_{34} - D_{35} - D_{36} + D_{37} + D_{38} - D_{39}], \quad (\text{A59})$$

where $D_0, D_{lm}, D_{lmn}(-p_2, p_4, p_3, m_b, m_k, m_k, m_k)$ are 4-point Feynman integrals

$$f_1^{b(m)} = 4m_t Q_b \sum_{k=\Pi_t^+, \Pi_a^+} q_k [-D_{27} - D_{311} + D_{313}], \quad (\text{A60})$$

$$f_2^{b(m)} = 0, \quad (\text{A61})$$

$$f_3^{b(m)} = Q_b \sum_{k=\Pi_t^+, \Pi_a^+} q_k [-2m_t^2 D_{12} + 2m_b^2 D_{12} + 2m_t^2 D_{13} - 2m_b^2 D_{13} - 4m_t^2 D_{24} + 4m_t^2 D_{25}]$$

$$\begin{aligned}
& -4D_{27} + 2m_t^2 D_{33} - 2m_t^2 D_{34} + 2m_t^2 D_{35} \\
& -2m_t^2 D_{39} - 8D_{312} + 8D_{313} \\
& +p_2 \cdot p_4 (4D_{22} - 4D_{26} + 4D_{36} - 4D_{310}) \\
& +p_1 \cdot p_2 (4D_{23} - 4D_{26} + 4D_{37} - 4D_{310}) \\
& +p_1 \cdot p_4 (-4D_{23} + 4D_{26} + 4D_{38} - 4D_{39}), \tag{A62}
\end{aligned}$$

$$f_4^{b(m)} = Q_b \sum_{k=\Pi_t^+, \Pi_a^+} q_k [-4D_{313}], \tag{A63}$$

$$\begin{aligned}
f_5^{b(m)} = Q_b \sum_{k=\Pi_t^+, \Pi_a^+} q_k [& 2m_t^2 D_{11} - 2m_b^2 D_{11} - 2m_t^2 D_{12} \\
& + 2m_b^2 D_{12} + 4m_t^2 D_{21} - 4m_t^2 D_{24} \\
& + 2m_t^2 D_{31} - 2m_t^2 D_{34} + 2m_t^2 D_{37} - 2m_t^2 D_{39} + 8D_{311} - 8D_{312} \\
& + p_2 \cdot p_4 (4D_{22} - 4D_{24} - 4D_{34} + 4D_{36}) \\
& + p_1 \cdot p_2 (4D_{25} - 4D_{26} + 4D_{35} - 4D_{310}) \\
& + p_1 \cdot p_4 (-4D_{25} + 4D_{26} + 4D_{38} - 4D_{310})], \tag{A64}
\end{aligned}$$

$$f_6^{b(m)} = -4Q_b \sum_{k=\Pi_t^+, \Pi_a^+} q_k [D_{27} + D_{311}], \tag{A65}$$

$$f_7^{b(m)} = 4m_t Q_b \sum_{k=\Pi_t^+, \Pi_a^+} q_k [-D_{23} + D_{26} + D_{33} - D_{37} - D_{39} + D_{310}], \tag{A66}$$

$$f_8^{b(m)} = 4m_t Q_b \sum_{k=\Pi_t^+, \Pi_a^+} q_k [-D_{25} + D_{26} - D_{35} + D_{37} - D_{39} + D_{310}], \tag{A67}$$

$$\begin{aligned}
f_9^{b(m)} = 4m_t Q_b \sum_{k=\Pi_t^+, \Pi_a^+} q_k [& D_{12} - D_{13} + D_{23} + 2D_{24} \\
& - 2D_{25} - D_{26} + D_{34} - D_{35} + D_{37} - D_{310}], \tag{A68}
\end{aligned}$$

$$\begin{aligned}
f_{10}^{b(m)} = 4m_t Q_b \sum_{k=\Pi_t^+, \Pi_a^+} q_k [& -D_{11} + D_{12} - 2D_{21} + 2D_{24} \\
& + D_{25} - D_{26} - D_{31} + D_{34} + D_{35} - D_{310}], \tag{A69}
\end{aligned}$$

$$f_{11}^{b(m)} = 4Q_b \sum_{k=\Pi_t^+, \Pi_a^+} q_k [D_{27} + D_{312}], \tag{A70}$$

$$f_{12}^{b(m)} = Q_b \sum_{k=\Pi_t^+, \Pi_a^+} q_k [-2D_{27}], \tag{A71}$$

$$f_{13}^{b(m)} = 2m_t Q_b \sum_{k=\Pi_t^+, \Pi_a^+} q_k [D_{12} - D_{13} + D_{23} + D_{24} - D_{25} - D_{26}], \tag{A72}$$

$$f_{14}^{b(m)} = 0, \quad (\text{A73})$$

$$f_{15}^{b(m)} = 2m_t Q_b \sum_{k=\Pi_t^+, \Pi_a^+} q_k [-D_{11} + D_{12} - D_{21} + D_{24} + D_{25} - D_{26}], \quad (\text{A74})$$

$$f_{16}^{b(m)} = 0, \quad (\text{A75})$$

$$f_{17}^{b(m)} = 4Q_b \sum_{k=\Pi_t^+, \Pi_a^+} q_k [D_{23} - D_{26} - D_{38} + D_{39}], \quad (\text{A76})$$

$$f_{18}^{b(m)} = 4Q_b \sum_{k=\Pi_t^+, \Pi_a^+} q_k [D_{25} - D_{26} - D_{38} + D_{310}], \quad (\text{A77})$$

$$f_{19}^{b(m)} = 4Q_b \sum_{k=\Pi_t^+, \Pi_a^+} q_k [-D_{22} + D_{26} - D_{36} + D_{310}], \quad (\text{A78})$$

$$f_{20}^{b(m)} = 4Q_b \sum_{k=\Pi_t^+, \Pi_a^+} q_k [-D_{22} + D_{24} + D_{34} - D_{36}], \quad (\text{A79})$$

where $D_0, D_{lm}, D_{lmn}(-p_2, p_4, -p_1, m_k, m_b, m_b, m_k)$ are 4-point Feynman integrals .

$$f^\Delta = \sum_{k=\Pi_t^+, \Pi_a^+} q_k [2m_t C_{11}(-p_2, p_4 + p_3, m_b, m_k, m_k)]. \quad (\text{A80})$$

$$f_{\mu\nu}^s = \sum_{k=\Pi_t^0, \Pi^0, \Pi^3} \frac{i\epsilon_{\mu\nu\rho\sigma} p_4^\rho p_3^\sigma}{\hat{s} - m_k^2 + im_k \Gamma_k} [8N_c Q_t^2 q_k m_t C_0(p_4, -p_4 - p_3, m_t, m_t, m_t) - \frac{c_t m_t' \mathcal{S}_{k\gamma\gamma}}{8e^2 \pi^2 f_\Pi^2}], \quad (\text{A81})$$

In the above:

$$Y_{\Pi_t^0} = Y_{\Pi_a^0} = Y_{\Pi_a^3} = -1, \quad Y_{\Pi_t^+} = Y_{\Pi_a^+} = 0 \quad (\text{A82})$$

$$m'_{\Pi_t^0} = m'_{\Pi_a^0} = m'_{\Pi_a^3} = m_t, \quad m'_{\Pi_t^+} = m'_{\Pi_a^+} = m_b$$

$$Q'_{\Pi_t^0} = Q'_{\Pi_a^0} = Q'_{\Pi_a^3} = Q_t, \quad Q'_{\Pi_t^+} = Q'_{\Pi_a^+} = Q_b$$

$$Q_t = \frac{2}{3}, \quad Q_b = -\frac{1}{3}, \quad N_c = 3 .$$

In WTC model:

$$q_{\Pi^0} = q_{\Pi^3} = q_{\Pi^+} = 0 , \quad (\text{A83})$$

$$q_{\Pi_a^0} = q_{\Pi_a^3} = q_{\Pi_a^+} = \frac{2m_t^2}{16\pi^2 f_\Pi^2} \frac{4}{3} , \quad (\text{A84})$$

$$q_{\Pi_t^0} = q_{\Pi_t^+} = 0 , \quad (\text{A85})$$

$$\mathcal{S}_{\Pi^0\gamma\gamma} = \mathcal{S}_{\Pi^3\gamma\gamma} = \mathcal{S}_{\Pi_t^0\gamma\gamma} = 0 . \quad (\text{A86})$$

In TOPCTC model:

$$q_{\Pi^0} = q_{\Pi^3} = q_{\Pi^+} = \frac{c_t^2 m_t'^2}{32\pi^2 f_{\Pi}^2}, \quad (\text{A87})$$

$$q_{\Pi_a^0} = q_{\Pi_a^3} = q_{\Pi_a^+} = \frac{2m_t'^2}{16\pi^2 f_{\Pi}^2} \frac{4}{3}, \quad (\text{A88})$$

$$q_{\Pi_t^0} = q_{\Pi_t^+} = \frac{(m_t - m_t')^2}{32\pi^2 f_{\Pi_t}^2}, \quad (\text{A89})$$

$$c_t = \frac{1}{\sqrt{6}}, \mathcal{S}_{\Pi^0\gamma\gamma} = -\frac{4e^2 N_{TC}}{3\sqrt{6}}, \mathcal{S}_{\Pi^3\gamma\gamma} = \frac{4e^2 N_{TC}}{\sqrt{6}}, \mathcal{S}_{\Pi_t^0\gamma\gamma} = 0. \quad (\text{A90})$$

In TOPCMTC model, the q_k s are the same as in (B) and

$$c_t = \frac{2}{\sqrt{6}}, \mathcal{S}_{\Pi^0\gamma\gamma} = \frac{10e^2 N_{TC}}{3\sqrt{6}}, \mathcal{S}_{\Pi^3\gamma\gamma} = \frac{2e^2 N_{TC}}{\sqrt{6}}, \mathcal{S}_{\Pi_t^0\gamma\gamma} = 0. \quad (\text{A91})$$

Reference

1. S. Weinberg, Phys. Rev. **D19**, 1277(1979); S. Dimopoulos and L. Susskind, Nucl. Phys. **B155**, 237(1979).
2. S. Dimopoulos and L. Susskind, Nucl. Phys. **B155**, 237(1979); E. Eichten and K. Lane, Phys. Lett. **B90**, 125(1980); E. Eichten, I. Hinchliffe, K. Lane, and C. Quigg, Rev. Mod. Phys. **56**, 579(1984).
3. B. Holdom, Phys. Rev. **D24**, 1441(1981); Phys. Lett. **B150**, 301 (1985); T. Appelquist and L. C. R. Wijewardhana, Phys. Rev. **D36**, 568 (1987); K. Yamawaki, M. Banda, and K. Matumoto, Phys. Rev. Lett. **56**, 1335(1986); T. Akiba and T. Yanagida, Phys. Lett. **B169**, 432(1986).
4. T. Appelquist and J. Terning, Phys. Lett. **B315**, 139(1993).
5. K. Lane and E. Eichten, Phys. Lett., **B222**, 274(1989); K. Lane and M. V. Ramana, Phys. Rev. **D44**, 2678(1991).

6. C. T. Hill, Phys. Lett. **B345**, 483(1995); K. Lane and E. Eichten, Phys. Lett. **B352**, 382(1995); G. Buchalla, G. Burdman, C. T. Hill and D. Kominis, Phys. Rev. **D53**, 5185(1996). FERMILAB-PUB-95/322-T.
7. F. Abe. et al., The CDF Collaboration, Phys. Rev. Lett. **74**, 2626(1995); S. Abachi, et al., The D0 Collaboration, Phys. Rev. Lett. **74**, 2697 (1995); G.F. Tartarelli, Fermilab Preprint CDF/PUB/TOP/PUBLIC/3664 (1996).
8. M. E. Peskin, in Physics and Experiments with Linear Collider, Proceedings of the Workshop, Saarikka, Finland, 1991, edited by R. Orava, P. Eerala and M. Nordberg (World Scientific, Singapore,1992)P.1.
9. For example, E. Malwaki and C.-P. Yuan, Phys. Rev. **D50**, 4462(1994); C.-P. Yuan, in Proc. of Workshops on Particles and Fields and Phenomenology of Fundamental Interactions, Puebla, Mexico, Nov. 1995; P. Haberl, O. Nachtmann, and A. Wilch, Phys. Rev. **D53**, 4875(1996); K. Cheung, Phys. Rev. **D55**, 4430(1997); F. Larios, E. Malwaki, and C.-P. Yuan, in *Physics at TeV Energy Scale*, CCAST-WL Workshop Series: Vol. **72**, 49(1996), edited by Y.-P. Kuang, and references therein.
10. J.H. Köhn, E. Mirkes, and J. Steegborn, Z. Phys. **C57**, 615(1993); O.J.P. Ébdi *et al.*, Phys. Rev. **D47**, 1889(1993); M. Drees, M. Krämer, J. Zunft, and P.M. Zerwas, Phys. Lett. **B306**, 371(1993).
11. A. Denner, S. Dittmaier and M. Stöckel, Phys. Rev. **D53**, 44(1996).
12. C.-S. Li, J.-M. Yang, Y.-L. Zhu, and H.-Y. Zhou, Phys. Rev. **D54**, 4662(1996); H. Wang, C.-S. Li, H.-Y. Zhou, and Y.-P. Kuang, Phys. Rev. **D54**, 4374(1996).
13. E. Eichten and K. Lane, Phys. Lett. **B327**, 129 (1994).
14. K. Lane, Phys. Lett. **B357**, 624(1995).

15. C.-X. Yue, H.-Y. Zhou, Y.-P. Kuang and G.-R. Lu, Phys. Rev. D**55**, 5541 (1997).
16. G. Passarino and M. Veltman, Nucl. Phys. **B160**, 151(1979); A. Axelrod, Nucl. Phys. **B209**, 349(1982); M. Clements et al., Phys. Rev. D**27**, 570(1983).
17. M.E. Peskin and T. Takeuchi, Phys. Rev. Lett. **65**, 964(1990).
18. See for instance, J. Ellis, M. K. Gaillard, D. V. Nanopoulos and P. Sikivie, Nucl. Phys. **B 182**, 529(1981); C.-X. Yue, Y.-P. Kuang G.-R. Lu, and L.-D. Wan, Phys. Rev. D**52**, 5314(1995).
19. O. J. P. Eholi, et al., Phys. Rev. D**47**, 1889(1993); King-Man Cheung, Phys. Rev. D**47**, 3750 (1993).
20. K. Hagiwara and D. Zeppenfeld, Nucl. Phys. **B313**, 560(1989); V. Barger, T. Han and D. Zeppenfeld, Phys. Rev. D**41**, 2782(1990).
21. A. Denner, Fortschr. Phys. **41** 307(1994).
22. W. Beenakker *et al.*, Nucl. Phys. **B411**, 343(1994).
23. The NLC ZDR Design Group and The NLC Physics Working Group, *Physics and Technology of the Next Linear Collider* (Report at Snowmass'96), BNL 52-502 Fermilab-PUB-96/112 LBNL-PUB-5425 SLAC Report 485 UCRL-ID-124160 UC-414.
24. B. Balaji, Phys. Rev. D**53**, 1699(1996).
25. S. Dimopoulos, S. Raby, and G.L. Kane, Nucl. Phys. **B182**, 77(1981); J. Ellis, M.K. Gaillard, D. V. Manopoulos and P. Sikive, Nucl. Phys. **B182**, 529(1981); V. Lubicz, Nucl. Phys. **B404**, 559(1993); V. Lubicz and P. Santorelli, Nucl. Phys.**B460**,3(1996). Preprint BUHEP-95-16.

26. S. Adler, Phys. Rev. **177**, 2426(1969); J.S. Bell and R. Jackiw, Nuo.Cim **60A**, 47(1969).
27. D. Slaven, Bing-Lin Young, and Xin-Min Zhang, Phys. Rev. D**45**, 4349 (1992).
28. S.J. Brodsky, P.M. Zerwas, Nucl. Instr. Meth. **A355**, 19 (1995).
29. T. Asaka, Y. Shobuda, Y. Sumino, N. Maekawa, and T. Moroi, in Proc. workshop on Physics and Experiments with Linear Collider, Morioka, Japan, 1995, edited by A. Miyamoto, y. Fujii. T. Matsui and S. Iwata (World Scietific Pub., Singapore, 1996), p.470; T. Askak, N. Maekawa, T. Moroi, Y. Shobuda, and Y. Sumino, Prog. Theore. Phys. Suppl. **123**, 151 (1996).
30. S. Dimopoulos, Nucl. Phys. **B168**, 69 (1980); L. Randall and E.H. Simmons, Nucl. Phys. **B380**, 3 (1992).
31. C.-X. Yue, Y.-P. Kuang, and G.-R. Lu, Z. Phys. **C76**, 133 (1997).

Table I. TC PGB corrections to the $\gamma\gamma \rightarrow t\bar{t}$ cross section $\Delta\sigma$, the relative correction $\Delta\sigma/\sigma_0$, and the total cross section $\sigma = \sigma_0 + \Delta\sigma$ for various values of m_{Π_a} in the Appelquist-Terning model ($\sigma_0 = 57.77$ fb for $\sqrt{s} = 0.5$ TeV, $\sigma_0 = 535.4$ fb for $\sqrt{s} = 1.5$ TeV).

m_{Π_a} (GeV)	$\sqrt{s} = 0.5$ TeV			$\sqrt{s} = 1.5$ TeV		
	$\Delta\sigma$ (fb)	$\Delta\sigma/\sigma_0(\%)$	σ (fb)	$\Delta\sigma$ (fb)	$\Delta\sigma/\sigma_0(\%)$	σ (fb)
250	-9.11	-15.8	48.66	-50.77	-9.5	484.6
275	-8.22	-14.2	49.55	-43.81	-8.2	491.6
300	-7.47	-12.9	50.30	-37.76	-7.1	497.6
325	-6.83	-11.8	50.94	-33.82	-6.3	501.6
350	-6.28	-10.9	51.49	-30.56	-5.7	504.8
375	-5.80	-10.0	51.97	-28.62	-5.3	506.8
400	-5.38	-9.3	52.39	-26.71	-5.0	508.7
425	-5.02	-8.7	52.75	-25.16	-4.7	510.2
450	-4.69	-8.1	53.08	-23.76	-4.4	511.6
475	-4.40	-7.6	53.37	-22.50	-4.2	512.9
500	-4.13	-7.1	53.64	-21.62	-4.0	513.8

Table II. Top-pion contributions from Fig.1(a)-(n) to the $\gamma\gamma \rightarrow t\bar{t}$ production cross section $\Delta\sigma$, the relative correction $\Delta\sigma/\sigma_0$ and the total production cross section $\sigma = \sigma_0 + \Delta\sigma$ in the original TOPCTC model ($\sqrt{s} = 0.5$ TeV).

m_{Π_t} (GeV)	$\Delta\sigma$ (fb)	$\Delta\sigma/\sigma_0(\%)$	σ (fb)
180	-13.04	-22.6	44.73
185	-9.81	-17.0	47.96
190	-8.05	-13.9	49.72
195	-7.27	-12.6	50.05
200	-7.22	-12.5	50.55
210	-7.86	-13.6	49.91
215	-7.83	-13.6	49.94
225	-7.57	-13.1	50.20
250	-6.73	-11.6	51.04
275	-5.97	-10.3	51.80
300	-5.35	-9.3	52.42

Table III. Total TC PGB and top-pion contributions from Fig.1(a)-(p) to the $\gamma\gamma \rightarrow t\bar{t}$ production cross section $\Delta\sigma$ and the total production cross section $\sigma = \sigma_0 + \Delta\sigma$ in the original TOPCTC model ($N_{TC} = 4$, $\sigma_0 = 57.77$ fb for $\sqrt{s} = 0.5$ TeV, $\sigma_0 = 535.4$ fb for $\sqrt{s} = 1.5$ TeV,).

m_{Π_t} (GeV)	$\sqrt{s} = 0.5$ TeV				$\sqrt{s} = 1.5$ TeV			
	$m'_t = 5$ GeV		$m'_t = 20$ GeV		$m'_t = 5$ GeV		$m'_t = 20$ GeV	
	$\Delta\sigma$ (fb)	σ (fb)	$\Delta\sigma$ (fb)	σ (fb)	$\Delta\sigma$ (fb)	σ (fb)	$\Delta\sigma$ (fb)	σ (fb)
180	-41.96	15.81	-38.53	19.24	-179.5	355.9	-154.7	380.7
200	-37.70	20.07	-35.13	22.64	-145.3	390.1	-125.3	410.1
225	-40.53	17.24	-38.04	19.73	-123.9	411.5	-108.2	427.2
250	-41.27	16.50	-39.68	18.09	-113.8	421.6	-99.3	436.1
275	-40.34	17.43	-40.87	16.90	-107.0	428.4	-96.1	439.3
300	-33.37	22.40	-38.97	18.80	-101.9	433.5	-94.2	441.2

Table IV. Total TC PGB and top-pion contributions from Fig.1(a)-(p) to the $\gamma\gamma \rightarrow t\bar{t}$ production cross section $\Delta\sigma$ and the total production cross section $\sigma = \sigma_0 + \Delta\sigma$ in the TOPCMTC model ($N_{TC} = 4$, $\sigma_0 = 57.77$ fb for $\sqrt{s} = 0.5$ TeV, $\sigma_0 = 535.4$ fb for $\sqrt{s} = 1.5$ TeV).

$\sqrt{s} = 0.5$ TeV								
m_{Π^0, Π^3}	$m'_t = 5$ GeV				$m'_t = 20$ GeV			
	$m_{\Pi_t} = 180$ GeV		$m_{\Pi_t} = 250$ GeV		$m_{\Pi_t} = 180$ GeV		$m_{\Pi_t} = 250$ GeV	
	$\Delta\sigma$ (fb)	σ (fb)	$\Delta\sigma$ (fb)	σ (fb)	$\Delta\sigma$ (fb)	σ (fb)	$\Delta\sigma$ (fb)	σ (fb)
100	-42.88	14.89	-41.35	16.42	-42.92	14.85	-41.30	16.47
150	-42.95	14.82	-41.33	16.44	-43.03	14.74	-41.12	16.65
200	-43.06	14.71	-41.29	16.48	-43.06	14.71	-40.63	17.14
250	-43.23	14.54	-41.17	16.60	-42.54	15.23	-39.07	18.70
300	-43.43	14.34	-40.51	17.26	-38.11	19.66	-32.19	25.58
325	-43.24	14.53	-39.30	18.47	-26.16	31.61	-17.22	40.55
$\sqrt{s} = 1.5$ TeV								
m_{Π^0, Π^3}	$m'_t = 5$ GeV				$m'_t = 20$ GeV			
	$m_{\Pi_t} = 180$ GeV		$m_{\Pi_t} = 250$ GeV		$m_{\Pi_t} = 180$ GeV		$m_{\Pi_t} = 250$ GeV	
	$\Delta\sigma$ (fb)	σ (fb)	$\Delta\sigma$ (fb)	σ (fb)	$\Delta\sigma$ (fb)	σ (fb)	$\Delta\sigma$ (fb)	σ (fb)
100	-201.2	334.2	-136.9	398.5	-218.3	317.1	-166.7	368.7
150	-201.8	333.6	-137.7	397.7	-218.3	317.1	-166.1	369.3
200	-203.4	332.0	-138.2	397.2	-219.3	316.1	-166.9	368.5
250	-204.3	331.1	-139.0	396.4	-220.0	315.4	-167.2	368.2
300	-206.7	328.7	-140.8	394.6	-219.9	315.5	-166.0	369.4
325	-207.1	328.3	-141.3	394.1	-212.7	322.7	-157.8	377.6

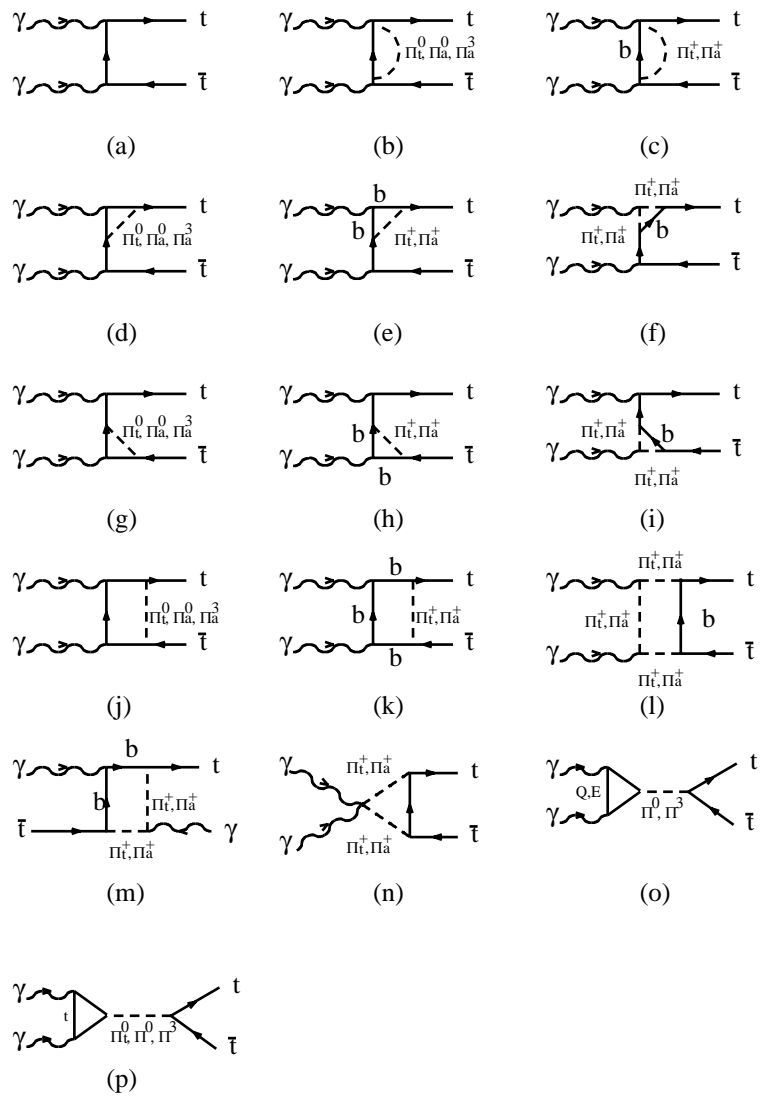


Fig.1

Fig. 1 Feynman diagrams for PGB contributions to the $\gamma\gamma \rightarrow t\bar{t}$ process. (a): tree level diagrams; (b)-(c): self-energy diagrams; (d)-(i): vertex diagrams; (j)-(m): box diagrams; (n): triangle diagram; (o)-(p): s -channel diagrams.

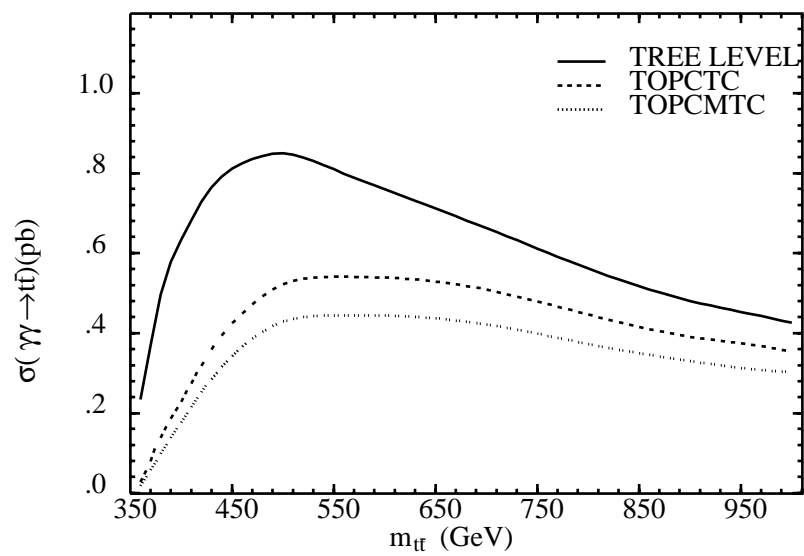


Fig. 2

Fig. 2 Subprocess cross sections $\sigma(\hat{s})$ in the tree level SM, the original TOPCTC model and the TOPCMTC model with $m_{\Pi_t} = 180$ GeV, $m_{\Pi^0, \Pi^3} = 100$ GeV and $m'_t = 20$ GeV.